Pharmaceutical Biology

Natural extracts into chitosan nanocarriers for rosmarinic acid drug delivery

Sara Baptista da Silva, Manuela Amorim, Pedro Fonte, Raquel Madureira, Domingos Ferreira, Manuela Pintado & Bruno Sarmento

📄 View supplementary material ↗

📅 Published online: 09 Dec 2014.

✎ Submit your article to this journal ↗

📊 Article views: 1589

🔍 View related articles ↗

✚ View Crossmark data ↗

🗐 Citing articles: 17 View citing articles ↗

ORIGINAL ARTICLE

Natural extracts into chitosan nanocarriers for rosmarinic acid drug delivery

Sara Baptista da Silva[1,2], Manuela Amorim[2], Pedro Fonte[3], Raquel Madureira[2], Domingos Ferreira[1], Manuela Pintado[2], and Bruno Sarmento[3,4]

[1]Department of Pharmaceutical Technology, Faculty of Pharmacy, University of Porto, Porto, Portugal, [2]CBQF, Biotechnology School, Portuguese Catholic University, Porto, Portugal, [3]Department of Pharmaceutical Sciences, IINFACTS, Institute of Health Sciences-North, CESPU, Gandra, Portugal, and [4]INEB, Institute of Biomedical Engineering, University of Porto, Porto, Portugal

Abstract

Context: Nanotechnology can be applied to deliver and protect antioxidants in order to control the oxidative stress phenomena in several chronic pathologies. Chitosan (CS) nanoparticles are biodegradable carriers that may protect antioxidants with potent biological activity such as rosmarinic acid (RA) in *Salvia officinalis* (sage) and *Satureja montana* (savory) extracts for safe and innovative therapies.

Objective: Development and characterization of CS nanoparticles as a stable and protective vehicle to deliver RA for medical applications using natural extracts as sage and savory.

Materials and methods: Antioxidant-CS based nanoparticles were prepared by ionic gelation with sodium tripolyphosphate (TPP), at pH 5.8 with a mass ratio of 7:1 (CS:TPP), with a theoretical antioxidant-CS loading of 40–50%. The nanoparticles were then characterized by different methods such as photon correlation spectroscopy, laser Doppler anemometry, scanning electron microscopy (SEM), differential scanning calorimetry (DSC), Fourier-transform infrared (FTIR), high-performance liquid chromatographic (HPLC), association efficiency, and antioxidant activity.

Results and discussion: Individual and small sizing nanoparticles, around 300 nm, were obtained. SEM confirmed smooth and spherical nanoparticles after freeze-drying. No chemical interactions were found between antioxidants and CS, after encapsulation, by DSC and FTIR. The association efficiency was 51.2% for RA (with 40% loading) and 96.1 and 98.2% for sage and savory nanoparticles, respectively (both with 50% loading). Antioxidant activity values were higher than 0.0348 eq [Asc. Ac.] g/L/g extract and 0.4251 µmol/eq Trolox/g extract.

Conclusion: The extracts under study are promising vehicles for RA drug delivery in CS nanocarriers.

Introduction

Salvia officinalis and *Satureja montana* (sage and savory, respectively) are plants often used in the traditional medicine to improve digestion (Gião et al., 2009), as an disinfectant (Djenane et al., 2011), to decrease blood pressure (Petersen & Simmonds, 2003), to prevent premature ejaculation (Zavatti et al., 2011), to treat neuropathy (Abada et al., 2011), urinary and pulmonary infections (Cardilea et al., 2009), and other diseases such as Alzheimer's disease (Zhoua et al., 2011) and cancer (Cardilea et al., 2009). Some of these biological activities have been associated with its high contents in RA (Gião et al., 2009; Shahidi et al., 1992; Skoula et al., 2000). RA (a-*O*-caffeoyl-3,4-dihydroxyphenillactic acid) is a phenolic compound generally admitted as a free radical scavenger (Fadel et al., 2011). The high biological activity is related to its chemical structure, in particular the two catechol moieties. Catechol is an important sub-structure for the potent antioxidant activity of phenolic antioxidants (Fadel et al., 2011). The general antioxidant mechanism of phenolic compounds is thought to be divided into two stages: radical catching stage and radical conclusion stage (Fujimoto & Masuda, 2012). The structure of the final product would afford important information about the antioxidant mechanism of the phenolics (Fujimoto & Masuda, 2012). RA can have many beneficial functionalities like its potent antioxidant activity associated to its huge potential radical scavenging activity, higher than trolox (a derivative of α-tocopherol), commonly used as a control. Its antibacterial and antiviral activity, anti-inflammatory activity (Huang et al., 2009), anti-mutagenicity character (Furtado et al., 2008), capability to reduce atopic dermatitis symptoms (Lee et al., 2008), prevention of Alzheimer's disease (Hamaguchi et al., 2009), and apoptosis induction of colorectal cancer cells (Xavier et al., 2009) are also well documented. Nevertheless, besides the lower partition coefficients and poor absorption that constrain the

Correspondence: Sara Baptista da Silva, Department of Pharmaceutical Technology, Faculty of Pharmacy, University of Porto, Rua Jorge Viterbo Ferreira 228, 4050-313 Porto, Portugal. Tel: +351 220 428 537. E-mail: sara.baptistadasilva@gmail.com

transport across biological barriers, most of the natural antioxidants or other active compounds are unstable and must be protected from degradation in the physiological environment (Hou et al., 2012). Thus, the efficacy of these drugs clearly depends on the design of appropriate carriers for their delivery, protection, and release (Prabaharan & Mano, 2005). Among the different approaches explored so far, colloidal carriers of particular interest, especially those made of mucoadhesive polymers, assure drug time retention at the absorption site (Campos et al., 2004). For this application, chitosan (CS) has become of particularly interesting for the association and delivery of labile macromolecular compounds (Silva et al., 2011). CS nanoparticle carriers have an exceptional potential for drug delivery, especially for mucosal, since these systems are stable in contact with physiological fluids and barriers, control drug release, and protect against adverse conditions like mucosal enzymes and biological protective fluids (Silva et al., 2011). The smart symbiosis of these CS nanoparticles with a high potent antioxidant could be a hope for future therapies, considering the important effect of oxidative stress in several chronic pathologies. In this study, CS nanoparticles were used, to incorporate natural extracts of *Salvia officinalis* and *Satureja montana* as a stable and protective vehicle to deliver RA for medical applications. There are no reports in the literature that have demonstrated the good performance of CS nanoparticles to incorporate these extracts in order to bring the huge benefits of RA antioxidant, as well as, other compounds that may act synergistically.

Materials and methods

Materials

The two selected plants sage and savory were provided by ERVITAL (Castro Daire, Portugal), from a previous study considering the potential antioxidant activity and the absence of genotoxicity of over 48 medicinal plants performed by our research group (Gião et al., 2007). The plants had been cultivated as organic products and were supplied in the commercial form of dried leaves. The dried leaves were then kept in the dark at 20 °C. RA (purity 96.5%), methanol CHROMASOLV® (HPLC ≥ 99.9%), and formic acid (HPLC ≥ 9 8.0%) were purchased from Sigma-Aldrich (Lisbon, Portugal). CS low molecular weight and sodium tripolyphosphate (TPP) were also purchased from Sigma-Aldrich (Lisbon, Portugal). The degree of deacetylation for the low molecular weight (LMW) CS was 85%, with a purity grade of 85%. Pure acetic acid was purchased from Pornalab (Lisbon, Portugal). Sodium hydroxide (NaOH) and hydrochloric acid (HCl) were from Merck (Darmstadt, Germany). Ultra-pure water was obtained in the laboratory using a Millipore™ water purification equipment (Millipore, Billerica, MA).

Sample preparation

The two plants, 1 g each, were crushed (using a lab mill) for 1 min, to obtain the corresponding powder. The extraction powder was performed as described in previous reports, via addition of 100 mL boiling water to 1 g of plant powder and after 5 min, the extract was filtered through a 0.45 μm filter (Silva et al., 2013). This procedure was optimized to obtain the highest potential activity of these plants. After the crude plant sedimentation, samples were filtered and maintained at −80 °C, for freeze-drying procedures (Heto Holten A/S Drywinner, Allerød, Denmark). Then, solutions of 1% (w/v) of freeze-dried powder were dissolved in methanol for chromatographic analyses and in ultra-pure water for antioxidant activity tests. Before injections, samples were filtered again through a 0.45 μm filter.

CS nanoparticles development and optimization

CS-nanoparticles were developed and optimized based on the previous studies. The CS nanoparticles were obtained by inducing the gelation of a CS solution with TPP. For this propose, TPP was dissolved in purified water, and CS was dissolved in acetic acid aqueous solutions at various concentrations and pH was adjusted to 5.8 with 1 M NaOH. The concentration of acetic acid was, in all cases, 1.75 times higher than that of CS, as previously described (Calvo et al., 1997). After several assays, considering the variation of concentrations and volumes, an optimal ratio between CS:TPP was achieved (7:1). This optimal ratio was considered to achieve particles ranging (200–300 nm) using ZetaPALS (Brookhaven Instruments Corp., New York, NY) and a charge as close as possible of 30 mV by laser Doppler anemometry (Brookhaven Instruments Corp., New York, NY), at 25 °C. A final volume of 2.0 mL of TPP solution was added to 5 mL of the CS solution under magnetic stirring at room temperature, thus achieving a final concentration of 2 and 0.28 mg/mL of CS and TPP, respectively.

Encapsulation of sage, savory, and rosmarinic acid into CS nanoparticles

The 1% (w/v) aqueous RA and aqueous extracts solutions were added to CS, previously dissolved in acetic acid, in different volumes in order to guarantee the best ratio between CS and the different compounds, as documented previously (Silva et al., 2013). For this concern, the encapsulation was tested in different theoretical loadings (5, 10, 15, 20, 30, 40, and 50%) fairly to the initial concentration of CS (2 mg/mL). All the tests were made for the seven batches, considering the two plants and the pure RA. Then, nanoparticles were freeze-dried and maintained at −20 °C for 1–2 months.

Association efficiency (AE)

AE was evaluated considering the amount of RA associated with the particles. For this propose, the particles were centrifuged (20 000 × g/45 min) and suspended in 7 mL of ultra-pure water. The AE was then calculated by the difference between the total RA used to prepare the particles and the amount of residual RA in the supernatant. AE of RA in RA nanoparticles and sage and savory nanoparticles were obtained according to the following equation:

$$\text{AE}\% = (\text{total amount} - \text{free amount}/\text{total amount}) * 100$$

In vitro release of rosmarinic acid from CS nanoparticles

The release of RA from CS nanoparticles was tracked to predict the diffusion and kinetic behavior of the nanosystems.

For release studies, loaded nanoparticles obtained after centrifugation were suspended in 10 mL of a phosphate-buffered saline (PBS) solution, pH 7.4. This nanoparticle suspension was transferred to clean eppendorfs and placed in a water bath at 37 °C under stirring. After 0.5, 1, 2, 4, 6, and 24 h, samples were collected from the bath and centrifuged at 14 000 rpm for 5 min (BOECO, Hamburg, Germany). Supernatants were analyzed by HPLC and used to calculate the amount of RA released from the nanoparticles over the specified time. Triplicate samples were analyzed at each time.

HPLC analysis and rosmarinic acid quantification

Chromatographic analysis was performed as described previously (Silva et al., 2013), using the Waters Series 600 HPLC and results acquired and processed with Empower® Software 2002 for data acquisition (Waters Corporation, Mildford, MA), on a Nova-Pack® RP C18 column (250 × 4.6 mm i.d., 5 μm particle size, and 125 Å pore size) from Waters Corporation (Mildford, MA), in a gradient mode with a mobile phase comprising methanol:formic acid:water 92.5:2.5:5 (v/v) at a flow rate of 0.75 mL/min. The injection volume was 20 μL and the detection wavelength was 280 nm. For analysis and quantification of RA content in the extracts, stock standard solutions of 2 mg/mL of RA were prepared with methanol. The calibration curve was made from the dilution of stock solutions in methanol of seven standard (0.05, 0.1, 0.2, 0.3, 0.5, 0.8, and 1) mg/mL. The HPLC method was validated according to the International Conference on Harmonization (ICH, 2005) guidelines.

Size and surface charge

Size and polydispersity (size distribution) of freshly unloaded and loaded nanoparticles were determined by photon correlation spectroscopy using ZetaPALS (Brookhaven Instruments Corporation, New York, NY). A sample of 1.6 mL was gently homogenized, placed into analyzer chamber, and measured. Collective six readings were performed three times on a sample of particles at 25 °C with a detection angle of 90°. The zeta potential (surface charge) was determined by laser Doppler anemometry (Brookhaven Instruments Corporation, New York, NY), at 25 °C. Triplicate samples were also analyzed, each sample being measured six times, and the arithmetic mean was adopted.

Morphology

Freeze-dried nanoparticles' morphology such as shape and occurrence of aggregation phenomena was studied by scanning electron microscopy (SEM). Samples of nanoparticles were mounted on metal stubs, gold coated under vacuum, and then examined on a JEOL-5600 Lv microscope (Joel, Tokyo, Japan). SEM was operated at the low vacuum mode, using a spot size of 27–28 and a potential of 30 kV. All analyses were performed at room temperature (20 °C).

Differential scanning calorimetry analysis

Thermograms were obtained using a differential scanning calorimetry (DSC) (DSC-60, Shimadzu, Columbia, MD). Samples were freeze-dried, and 2.0 mg of the freeze-dried powder were crimped in a standard aluminum pan and heated from 20 to 350 °C at a heating constant rate of 10 °C/min under constant purging of nitrogen at 20 mL/min. All samples were run in triplicate and data presented are the average of the three measurements.

Fourier-transform infrared analysis

Infrared spectroscopy analysis was performed in a ABB MB3000 FTIR spectrometer (ABB, Zurich, Switzerland) equipped with a horizontal attenuated total reflectance (ATR) sampling accessory (PIKE Technologies, Madison, WI), the Horizon MBTM FTIR software and a diamond/ZnSe crystal. All spectra were acquired using 200 scans and a 4 cm^{-1} resolution in the region of 4000–700 cm^{-1}. In order to perform the spectra comparison, spectra were truncated at 1800 and 700 cm^{-1}, since this region displays typical absorption bands for the used compounds. In addition, baseline-point adjustment and spectra normalization were performed. All samples were run in triplicate and data presented are the average of the three measurements.

Antioxidant capacity assessment

ABTS

Determination of the antioxidant capacity was performed as described in other research papers (Gião et al., 2007). The ABTS$^{\bullet}$+ stock solution was prepared via addition, at 1:1 (v/v), of 7 mM ABTS (2,2-azinobis (3-ethylbenzothiazoline-6-sulfonic) acid) diammonium salt (Sigma-Aldrich, St. Louis, MO) to a solution of 2.45 mM potassium persulfate (Merck, Darmstadt, Germany); the developing reaction took place in the dark, for 16 h. In order to obtain an absorbance of 0.700 ± 0.020 at 734 nm, measured with an UV 1203 spectrophotometer (Shimadzu, Tokyo, Japan), the aforementioned stock solution was diluted in ultra-pure water as necessary. A 10 μL aliquot of the sample was assayed for percentage of inhibition (PI), to be between 20% and 80%, to guarantee a linear response of the analytical method, after 6 min of reaction with 1 mL of diluted ABTS$^{\bullet}$+ solution.

The total antioxidant capacity was expressed as percentage of inhibition (PI), according to the equation:

$$PI = \left(AbsABTS^{\bullet} + -Abs\ sample \right)/AbsABTS^{\bullet}+) \times 100$$

where AbsABTS$^{\bullet}$+ denotes the initial absorbance of diluted ABTS$^{\bullet}$+, and Abs sample denotes the absorbance of the sample by 6 min of reaction. Triplicates of each sample were averaged to generate each datum point (which implies a total of six replicates per sample). The final result was expressed as an equivalent concentration of ascorbic acid (in gL^{-1}), using a calibration curve.

Oxygen radical absorbance capacity (ORAC)

The ORAC assay was employed to evaluate the antioxidant potential of CS-antioxidant nanoparticles as described previously in reports (Contreras et al., 2011). All reaction mixtures were prepared in duplicate, and at least three independent measures were performed for each experiment. ORAC-fluorescein (FL) values were expressed in μmol trolox

equivalent per mg hydrolyzed of antioxidant, as proposed elsewhere (Hernández-Ledesma et al., 2005).

Statistical analysis

Statistical analysis was performed using IBM SPSS Statistics v 19.0.0 (SPSS Inc., Chicago, IL). The one-way analysis of variance (ANOVA) was used with Scheffé *post hoc* test comparison of groups with normal distribution, and the Mann–Whitney test for groups with non-normal distribution. Differences were considered to be significant at a level of $p < 0.05$.

Results and discussion

Particle size, polydispersity, and zeta potential

Particle size and size distribution are important parameters towards the development of suitable nanomedicines for therapeutic purposes. They influence *in vivo* distribution, biological fate, toxicity, and the targeting ability of nanoparticle systems (Kumari et al., 2010). In addition, they can also influence the drug loading, drug release, and stability of drug inside nanoparticles (Mohanraj & Chen, 2006). Considering the nanoparticles' charge, it is known that the highest value of zeta potential represents the greater electrostatic repulsive interactions among the particles, the stability will increase as well as the size distribution will be more homogenous. Zeta potential values of ± 30 mV indicate that the colloidal system is stable in time and that amino groups of CS are on the surface, which is also documented in some similar studies of antioxidants encapsulation in CS nanoparticles (Harris et al., 2011). The loaded nanoparticles under study, ranging from 200 to 300 nm, and with zeta potential from 20 to 30 (Table 1) showed no significant differences ($p < 0.05$) between the different theoretical loadings for each formulation and between the two crude extracts, which is in accordance with the previous reports (Silva et al., 2013). RA-nanoparticles at 50% theoretical loading were the only exception, since their higher size (1218.0 ± 136.2) is not in the range of nano-scale and, as a consequence, not considered for the following tests. The extracts do not seem to interfere in the size or zeta potential of the nanoparticles being a good vehicle for RA nano-incorporation. The obtained nanoparticles also showed values of polydispersity between 0.1 and 0.2 corresponding to a narrow particle size distribution, and to monodispersed particles. These results are in accordance with other research works using similar antioxidant nanoparticles (Liu et al., 2011).

Morphology

SEM images can directly provide information on the particle size and morphology of nanoparticles. In this study, SEM images were analyzed to prove that the size was maintained after freeze dried (dehydration process). Figure 1 shows the SEM images of freeze-dried CS nanoparticles prepared by ionic gelation under the same pH conditions, for the encapsulation of RA in a pure form, sage and savory. The freeze-dried samples even with some aggregation of the nanoparticles formed by dispersion during freeze drying guarantee the nano-scale particles with the diameters under 1 μm, which is in accordance with other previous studies (Wu et al., 2012). The microstructural analysis confirmed the morphology and size of the nanoparticles. Other studies

Table 1. Zetasizer measurements and the association efficiency considering the different loading (%) of RA, sage, and savory nanoparticles ($n = 3$).

		Size and surface charge			Association efficiency		
Nano	Loading (%)	Size (nm)	Polydispersity	Zeta potential (mV)	Free amount concentration (μg/mL)	Total amount concentration (μg/mL)	Association efficiency (%)
RA	5	230.0 ± 48.8^a	0.155 ± 0.043	23.9 ± 5.5^b	56.6 ± 3.6	100	43.4 ± 3.5^c
	10	242.4 ± 112.3^a	0.215 ± 0.126	18.7 ± 2.3^b	94.8 ± 6.1	200	52.6 ± 3.1^c
	15	229.5 ± 40.1^a	0.142 ± 0.076	29.9 ± 9.9^b	147.9 ± 54.8	300	50.7 ± 18.3^c
	20	231.1 ± 68.3^a	0.149 ± 0.044	32.7 ± 6.4^b	186.4 ± 52.0	400	53.4 ± 2.0^c
	30	261.8 ± 50.4^a	0.171 ± 0.027	34.5 ± 4.5^b	306.0 ± 39.2	600	49.0 ± 6.5^c
	40	244.0 ± 18.0^a	0.193 ± 0.062	29.5 ± 1.6^b	390.4 ± 41.0	800	51.2 ± 3.0^c
	50	1218.0 ± 136.2^a	0.294 ± 0.132	35.0 ± 7.9^b	422.0 ± 65.0	1000	57.8 ± 1.3^c
Sage	5	330.9 ± 78.9^a	0.137 ± 0.012	20.8 ± 0.6^b	15.1 ± 0.4	100	84.9 ± 0.4^d
	10	224.3 ± 82.1^a	0.182 ± 0.061	24.3 ± 0.2^b	17.6 ± 0.6	200	91.2 ± 0.3^d
	15	200.0 ± 15.3^a	0.145 ± 0.018	21.4 ± 1.1^b	22.5 ± 1.1	300	92.5 ± 0.4^d
	20	243.0 ± 66.2^a	0.170 ± 0.123	21.7 ± 0.1^b	26.0 ± 4.0	400	93.5 ± 1.0^d
	30	271.5 ± 22.3^a	0.180 ± 0.056	27.8 ± 0.6^b	29.4 ± 3.0	600	95.1 ± 0.5^d
	40	272.9 ± 58.1^a	0.254 ± 0.099	25.1 ± 0.0^b	39.2 ± 2.1	800	95.1 ± 0.3^d
	50	278.4 ± 42.2	0.268 ± 0.092	24.9 ± 0.1^b	39.0 ± 2.6	1000	96.1 ± 0.2^d
Savory	5	233.1 ± 40.8^a	0.171 ± 0.083	23.8 ± 1.5^b	11.9 ± 0.0	100	88.1 ± 0.0^d
	10	230.7 ± 21.2^a	0.136 ± 0.094	27.8 ± 4.2^b	12.0 ± 0.1	200	94.0 ± 0.1^d
	15	182.7 ± 24.1^a	0.087 ± 0.075	28.0 ± 5.8^b	12.6 ± 0.1	300	95.8 ± 0.0^d
	20	220.8 ± 52.7^a	0.092 ± 0.024	26.7 ± 1.3^b	13.2 ± 0.2	400	96.7 ± 0.0^d
	30	188.0 ± 50.6^a	0.098 ± 0.006	28.9 ± 4.5^b	14.4 ± 0.6	600	97.6 ± 0.1^d
	40	139.4 ± 16.2^a	0.135 ± 0.088	28.4 ± 1.6^b	15.2 ± 0.4	800	98.1 ± 1.1^d
	50	229.3 ± 29.6^a	0.149 ± 0.121	26.5 ± 3.5^b	18.0 ± 0.2	1000	98.2 ± 0.1^d

[a,b]The results are given as mean of triplicate samples, each with six measurements. The same letters, in the same column indicate that no significant differences were observed between the values ($p < 0.05$).
[c,d]The results are given as mean of triplicate samples injections. The same letters, in the same column indicate that no significant differences were observed between the values ($p < 0.05$).
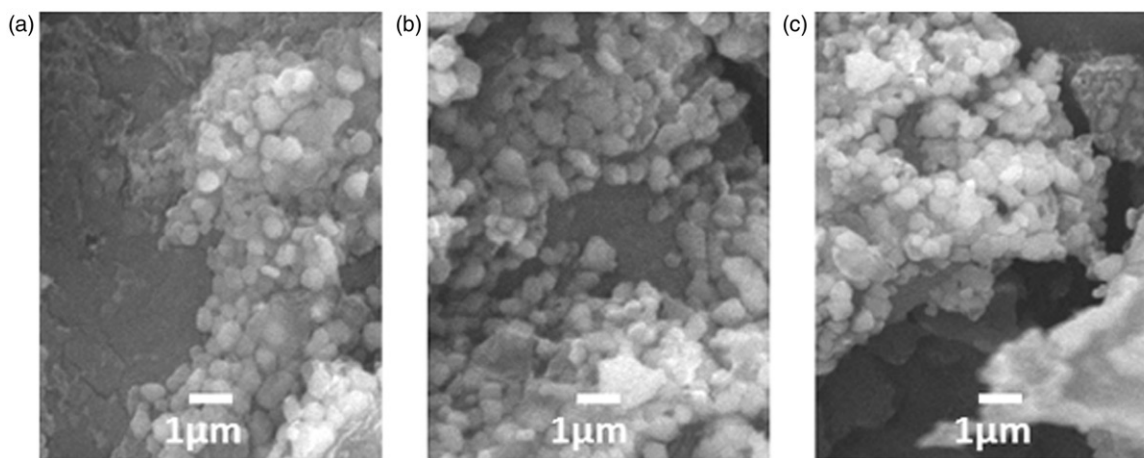
Figure 1. SEM micrographs of freeze-dried sage (a), savory-nanoparticles (b) both at 50% theoretical loading; and RA-nanoparticles (c), at 40% theoretical loading.

reported an increase in the particle size after freeze-drying with the unmodified CS particles (Dudhania & Kosarajua, 2010). This was resulted from aggregation from the strong inter- and intra-molecular hydrogen bonding, which was not possible to breakdown even by vortex homogenization (Dudhania & Kosarajua, 2010). This particles' size increase after freeze-drying process is also reported in essential oil encapsulation (Wu et al., 2012).

Association efficiency and drug loading

It is known that CS in acidic media (pKa 6.5) can interact with the negatively charged TPP, forming inter- and intra-molecular cross-linkages, yielding ionically cross-linked CS nanoparticles (Alonso & Sanchéz, 2003). This is a spontaneous method for smaller nanoparticles formation with positive charge, without using any organic solvent or surfactants (Dudhania & Kosarajua, 2010). It is also known that the inter- and intra-molecular linkages created between TPP and the positively charged amino groups of CS are responsible for the success of the gelation process (Calvo et al., 1997). In the present study, it was described as a nanoparticulate system able to encapsulate natural extracts. The particle size was observed to be dependent on both CS and TPP concentrations as described in the previous studies (Calvo et al., 1997), being the minimum sizes obtained for the lowest CS and TPP concentrations. Further experiments were conducted using the mass ratio CS:TPP of 7:1, where the TPP final concentration was 0.28 mg/mL and the CS final concentration was 2 mg/mL. RA was selected as a model antioxidant in order to investigate the feasibility of using CS and CS nanoparticles for natural extract carriers. Association efficiency and theoretical antioxidant loading of these nanoparticles are displayed in Table 1.

The pH of the nanoparticles formation medium was between 5.8 and 6.0, a pH value that favors the interaction of RA and CS, thus reaching a maximum leading to the entrapment of high amounts of RA. Among the different samples considering the encapsulation of RA into CS nanoparticles, it was observed similar association efficiency around 50% (Table 1), for all the different loadings, no significant differences were observed ($p < 0.05$). Higher

Table 2. Association efficiency, theoretical loading, and final RA content in CS nanoparticles.

Nano	Association efficiency (%)	Theoretical loading (%)	Final content in the CS nanoparticles (µg/mL)	Final RA content in CS nanoparticles (mg/mL)
RA	51.2 ± 3.0	40	800	400
Sage	96.1 ± 0.2	50	1000	100
Savory	98.2 ± 0.1	50	1000	50

association efficiency was found for RA entrapment in extracts of sage and savory, 96 and 98%, respectively, with no significant differences observed ($p < 0.05$). This was in accordance with previous reports (Silva et al., 2013). The higher association efficiency in extracts nanoparticles may be due to the different amounts of RA in CS nanoparticles inside the extracts in CS nanoparticles (Table 2). Since competitive interaction may be happen between phenolic (OH−) of RA and ($P_3P_3O_{10}^{5-}$) groups of TPP for protonated amino groups of CS resulting in low levels of particle formation compared with the CS nanoparticles, this may be intensified with the highest amount of RA and phenolic groups (Dudhania & Kosarajua, 2010). This is in accordance with other studies that encapsulate other phenolic compound, such as cathechin, in CS nanoparticles (Dudhania & Kosarajua, 2010) and in other nanoparticles (Peres et al., 2011).

The association efficiency values were higher than the results for other natural extracts encapsulated into CS nanoparticles, where the entrapment in CS-coated particles was lower (around 50%) since active compound was lost during immersion in CS (Deladino et al., 2008). This may be due to the huge affinity of CS and two crude extracts. The results were also higher than a study reported for quercitrin encapsulation into nanoparticles, which was only 40% (Kumari et al., 2011). However, the high association efficiency reported in this study was in accordance to other previous studies with the encapsulation of natural antioxidants extracted from *Ilex paraguariensis* into CS nanoparticles (Harris et al., 2011) and for the encapsulation of antioxidant idebenone loaded into CS nanoparticles (Amorim et al., 2010).

In vitro rosmarinic acid release from CS nanoparticles

A fast release was observed during the *in vitro* release assays which are in accordance with previous data (Silva et al., 2013). The different RA antioxidant contents (in RA nanoparticles, sage and savory nanoparticles) were released in all the formulations freshly and freeze-dried within 60 min with no significant differences ($p < 0.05$). An initial burst effect was observed in the first 30 min with approximately 80% in sage nanoparticles and 100% in RA and savory nanoparticles (in Supplemental information). The results seem to demonstrate that a significant amount of RA or extracts are initially associated with nanoparticles on their surfaces by weak linkages to CS, which did not have the necessary strength to entrap all the compounds. This represents that CS nanoparticulate system could retain the primary structure of RA or extracts during encapsulation. The protection release happens only for few minutes due to the polymer network, which is in accordance with other studies that encapsulate polyphenols from *Ilex paraguariensis* in CS nanoparticles prepared also by ionic gelation, and a complete release of 100% was demonstrated in the first 15 min (Harris et al., 2011). In another study for quercetin encapsulation into other nanocarriers, the release within the first 20 min was also 95% (Wu et al., 2008). Nevertheless, these results are different from other works that demonstrates a complete release of polyphenols of CS nanoparticles within 4 h (Dudhania & Kosarajua, 2010). The efficient application of these nanocarriers will certainly depend on the drug propose. CS nanoparticles maintain their characteristics for these theoretical loadings, and this confers them valuable properties, such as protective and moisturizer, for the encapsulation of active agents for cosmetic or ocular applications, since a rapid released is intentional (Harris et al., 2011). However, for other applications, like oral drug delivery, a slower release should be optimized.

Thermal behavior by DSC analysis

The DSC measurements provide quantitative and qualitative information about physical and chemical changes that involve endothermic or exothermic processes, or changes in heat capacity. Endothermic and exothermic peaks correspond to transitions that absorb or release energy. DSC was performed to understand the behavior of RA, sage and savory loaded and unloaded CS nanoparticles and the thermograms are displayed in Table 3.

The same CS nanoparticles' thermal behavior is observed in all thermograms (Figures 2Ia and IIa and 3IIIa). In all CS curves, an endothermic peak near 70 °C can be ascribed to the loss of water as reported previously (Guinesi & Cavalheiro, 2006). The endotherm of RA and sage and savory nanoparticles showed different shift temperatures (Figure 2Id, IId and IIId, respectively). This may be accounted for the hydrophilic groups incorporated due to RA that is in different amounts inside the extract particles. Other previous studies also reported similar shifts in DSC plots of CS and CS nanoparticles (Dudhania & Kosarajua, 2010; Vikas et al., 2004). It could also be seen that the peaks of the complexes were shifted from those of physical mixture. Peaks of physical mixture (Figure 2Ic, IIc, and IIIc) appeared

Table 3. Peak temperatures in the DSC thermograms collected from CS, RA, sage and savory, physical mixtures, and nanoparticles.

	T (°C)		
	Onset	Peak	EndSet
Nanos			
CS	102 ± 0.55	122 ± 1.20	131 ± 0.12
RA	112 ± 0.61	130 ± 0.73	141 ± 0.24
Sage	83 ± 0.27	108 ± 0.71	118 ± 0.93
Savory	103 ± 1.11	124 ± 0.82	137 ± 0.44
Free			
RA	134 ± 0.13	144 ± 0.23	149 ± 0.25
Sage	140 ± 0.21	141 ± 0.14	145 ± 1.03
Savory	141 ± 0.53	154 ± 0.51	158 ± 0.81
Physical mixture			
CS-RA	90 ± 0.38	122 ± 0.83	136 ± 0.14
	147 ± 0.14	150 ± 0.70	154 ± 0.13
CS-sage	94 ± 0.91	121 ± 0.10	134 ± 0.50
	147 ± 0.67	151 ± 0.63	155 ± 0.84
CS-savory	93 ± 0.70	121 ± 0.32	132 ± 0.32
	145 ± 0.28	151 ± 0.64	154 ± 0.24

to be combinations of each material but they are different from those of nanoparticles, probably because complexation of polyelectrolytes, in accordance with other similar works (Sarmento et al., 2006). Also, comparing endothermic peak of antioxidant-loaded CS nanoparticles to the one obtained with unloaded nanoparticles, the former started at higher temperature, which is a possible evidence of the presence of antioxidants, once its decomposition started at higher temperature when comparing with unloaded nanoparticles. The RA-, sage- and savory-loaded sample showed a similar shift of CS nanoparticles, which confirms that there are no significant covalent interactions between antioxidants and CS after encapsulation and cross-linking (Sarmento et al., 2006).

Fourier-transform infrared analysis

Structural features and functional groups that represent backbone produce characteristic and reproducible absorptions in the spectrum, which can be analyzed by FTIR. With these series of experiments, it was intended to monitorize the complexation of contrary charged polyelectrolytes at specific pH and stoichiometric relationship between the polyelectrolytes and the antioxidants in nanocarriers. For this concern and to examine this relationship between components of nanoparticulate systems, preliminary concerns were taken over polyelectrolyte interactions and antioxidants' entrapment. It is well established that the carboxyl group (–COO) of the anionic polymer may interact with the amino group ð-NH3 of CS and forms an ionic complex between the two compounds (Sarmento et al., 2006). RA displays a typical vibrational absorption bands with the main bands located between 1800 and 700 cm^{-1} (Stehfest et al., 2004). The three bands around 1605, 1520, and 1445 cm^{-1} are due to the presence of aromatic rings in the molecule indicating an aromatic ring stretching (Stehfest et al., 2004). Other evidences for phenolic groups were delivered through the bands at 1360 and 1180 cm^{-1} resulting from O–H and C–O stretches (Stehfest et al., 2004). Therefore, the band at 1684 cm^{-1} and the two shoulders recognized with this band

Figure 2. I. Thermogram of CS empty
nanoparticles (a); thermogram of free RA
(b); thermogram of RA and CS physical
mixture (mixing ratio 1:1) (c); thermogram of
RA encapsulated in CS nanoparticles (at a
theoretical 40% loading) (d). II. Thermogram
of CS empty nanoparticles (a); thermogram
of free sage (b); thermogram of sage and CS
physical mixture (mixing ratio 1:1) (c);
thermogram of sage encapsulated in CS
nanoparticles (at a theoretical 50% loading)
(d). III. Thermogram of CS empty nanopar-
ticles (a); thermogram of free savouy (b);
thermogram of savory and CS physical mix-
ture (mixing ratio 1:1) (c); thermogram of
savory encapsulated in CS nanoparticles (at a
theoretical 50% loading) (d).
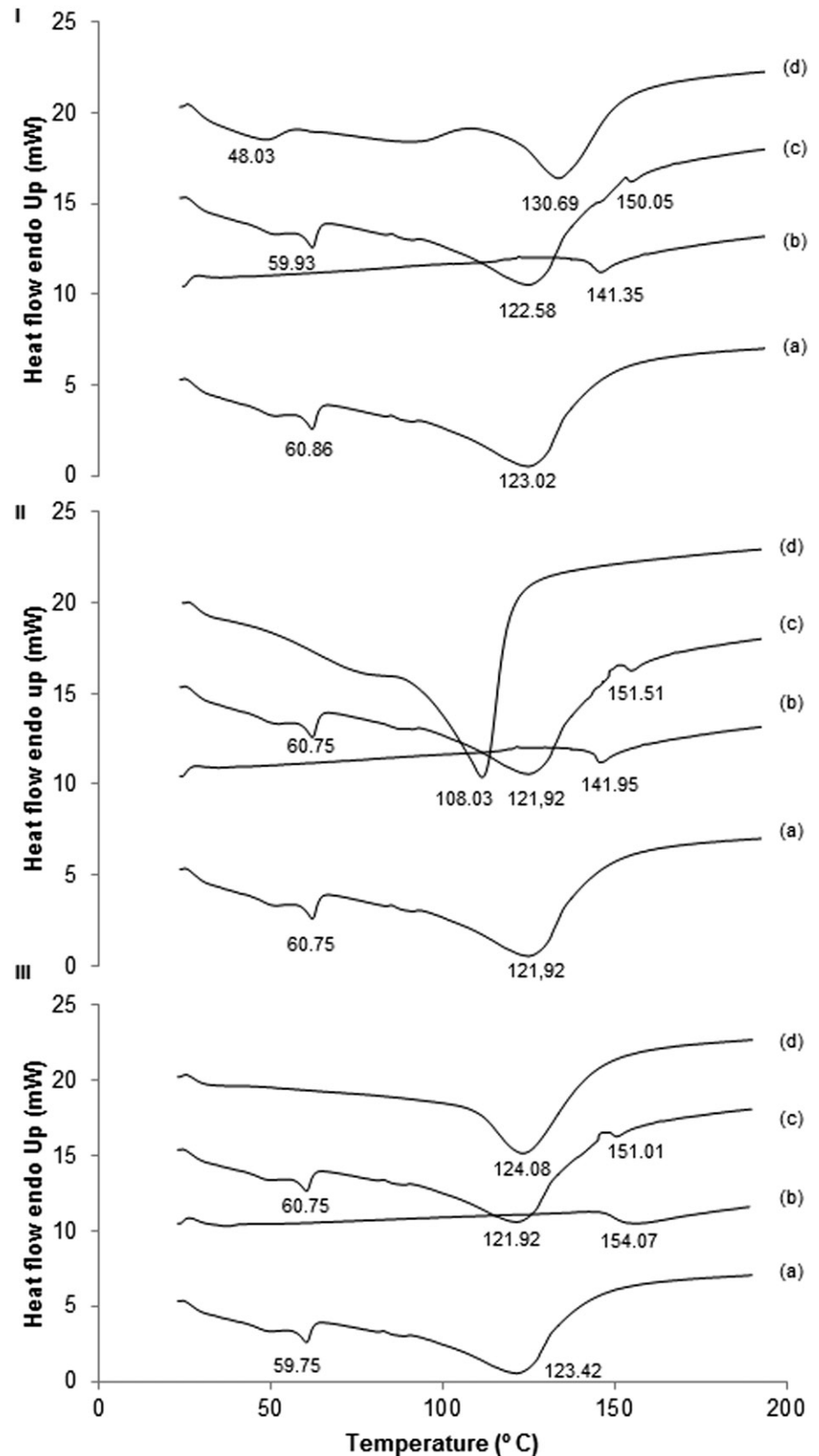
result probably from the shifted bands due to the presence of carboxylic acid groups and ester group 1725–1750 cm^{-1} (Roeges, 1995). Figure 3 (I, II, and III) shows that all the above characteristic peaks appear in the spectra of combined drugs-loaded CS nanoparticles at the same wavenumber indicating no modification or interaction between the drug and the carrier. This is in accordance to previous work (Ajun et al., 2009). Nevertheless, some peaks clearly decreased in intensity, after the preparation of RA, sage and savory nanoparticles. Particularly evident are the phenolic group bands (1360 and 1180 cm^{-1}) in RA nanoparticles and this is may be due to the highest amount of RA in these

Figure 3. I. Spectrum of CS empty nanoparticles (a); spectrum of RA in a free form (b); spectrum of physical mixture between CS-unloaded nanoparticles and RA (mixing ratio 1:1) (c); spectrum of RA encapsulation into CS nanoparticles (d). II. Spectrum of CS empty nanoparticles (a); spectrum of sage in a free form (b); spectrum of physical mixture between CS unloaded nanoparticles and sage (mixing ratio 1:1) (c); spectrum of sage encapsulation into CS nanoparticles (d). III. Spectrum of CS empty nanoparticles (a); spectrum of savory in a free form (b); spectrum of physical mixture between CS-unloaded nanoparticles and savory (mixing ratio 1:1) (c); spectrum of savory encapsulation into CS nanoparticles (d).
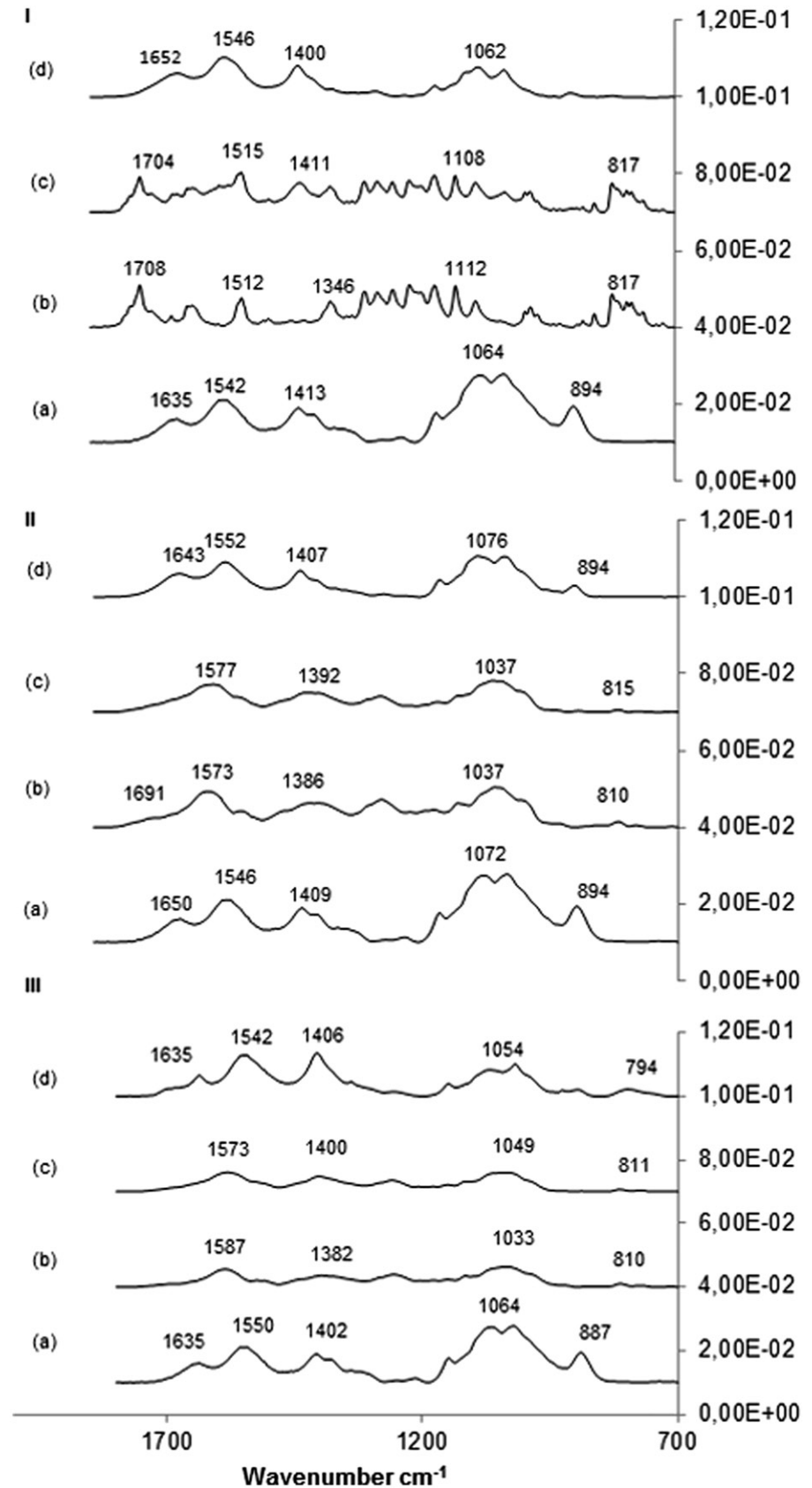
nanoparticles, comparing with the inside content of RA in extracts and nanoparticles. This effect is also reported by some authors that developed a new FTIR method for the characterization of RA in *Lavandula officinalis* cultures (Stehfest et al., 2004). Nevertheless, it must be underlined that this characteristic bands decrease observed in the nanoparticles by FTIR analysis, and the decrease in antioxidant activity (Antioxidant activity measurement section), may be due to the partial retention of antioxidant before their complete release (considering the theoretical loadings under studied). This is

Table 4. Antioxidant activity measurements by ABTS and ORAC, considering the 50% loading (m/m) sage and savory nanoparticles; and 40% loading (m/m) of and RA nanoparticles for ($n = 3$).

	ABTS[x] (eq [Asc. Ac.]g/L)/g extract		ORAC[y] (μmol/eq Trolox)/g extract	
	Fresh nanoparticles	Freeze-dried nanoparticles	Fresh nanoparticles	Freeze-dried nanoparticles
Nano[I]				
RA	0.0348 ± 0.0050^a	0.0554 ± 0.0139^a	4.8374 ± 0.1719^b	3.6520 ± 0.1770^b
Sage	0.0537 ± 0.0015^c	0.0440 ± 0.0029^c	0.6227 ± 0.0901^d	0.4251 ± 0.0069^d
Savory	0.0828 ± 0.0102^e	0.0378 ± 0.0015^f	1.5315 ± 0.2784^g	0.4526 ± 0.0087^h
Free[II]				
RA	0.0917 ± 0.0018		34.1218 ± 2.5733	
Sage	0.1621 ± 0.0470		19.5924 ± 1.9791	
Savory	0.1410 ± 0.0087		16.8117 ± 1.3605	

The results are given as mean of triplicate samples, each with three measurements. The same letters, in the same line indicate that no significant differences were observed between the fresh and freeze-dried process ($p < 0.05$). The values are significantly different ($p < 0.05$) for the antioxidant methods ([x, y]) and for the encapsulation process ([I, II]).

documented for other antioxidant nanoparticles studies, such as essential oils (Wu et al., 2012). Also no new peaks appeared in nanoencapsulation spectrum, and CS, RA, sage and savory were mixed together physically without any chemical reaction (Kumari et al., 2011).

Antioxidant activity measurement

For both methods, no significant differences were found for antioxidant activity between the nanoformulations, before and after freeze-drying processes ($p < 0.05$), except for savory encapsulation. For these nanoparticles, a decrease in the antioxidant activity was observed after freeze-drying, especially evident in the ORAC method. For the loading concentrations of 5–15%, no antioxidant activity was found by the ABTS or ORAC methods. This means that the antioxidant activity is clearly compromised for these low theoretical loadings. Considering both the extracts and RA nanoparticles, the highest antioxidant activity is correlated to the highest antioxidants concentrations (or higher % of loading) (Table 4). Comparing RA, sage and savory in a free form, it can be easily observed that RA has the highest antioxidant activity, followed by sage that has the highest content of RA (10%) and then savory with only (5%) of RA content (Table 4). By the ABTS method, comparing the antioxidant activity before and after the encapsulation process, it is clear a decrease in the antioxidant activity after the encapsulation. This proofs that the antioxidant activity was decreased due to the partial entrapment effect of the compounds. Nonetheless the particles still demonstrated good antioxidant activity. This is in accordance to other previous reports that have showed the same good antioxidant effect of trolox in CS nanoparticles (Han et al., 2012). Other good results were obtained for the CS encapsulation of idebenone antioxidant (Amorim et al., 2010). Furthermore and by ORAC, which is fluorimetric assay and a more sensitive one, it can be easily observed that after the encapsulation process the antioxidant activity is even lower than the results achieved by ABTS (Table 4). These results are in accordance with the previous studies with the encapsulation of quercetin and rutin (Coneaca et al., 2009). This still may be due to the nanoparticles entrapment of RA, in other way, the antioxidant was not completely released. This partial

retention means that the compounds will take more time to build up their specific activity. Nevertheless the nanosystems with this entrapment effect still have good antioxidant activity. Although even if the nanosystem antioxidant activity is lower than the unloaded compounds, it is well known that nanocarriers protect the antioxidants for degradation by biological and enzymatic fluids, increasing their bioavailability. The drug release can also be optimized to be even longer, prolonged, and controlled in time, considering the proposed application of these nanoparticles (Silva et al., 2011). This makes the nanoencapsulation advantageous and necessary.

Besides no significant differences ($p < 0.05$) were achieved in the all encapsulation process, and considering the same loading concentrations of the RA and the extract nanoparticles, it is also clear that RA in the extract nanoparticles is lower in concentration than when it is purely encapsulated. RA nanoparticles (40% loading) with 50% efficiency means encapsulate, 0.4 mg/mL of RA. Nevertheless, sage or savory nanoparticles (50% loading), with almost 100% association efficiency (Table 1), the nanosystem encapsulates 1 mg/mL of extract, but only 10 and 5% of RA (Table 2), for sage and savory, respectively. It is also known and documented by our group (Gião et al., 2009) that these crude extracts (sage and savory) are complex natural matrixes with different antioxidant contents (as protocatechuic acid, coumaric acid, gallic acid, caffeic acid, ferulic acid, naringenin, quercetin, isorhamnetin, chlorogenic acid, prunin, isoorientin, quercitrin, and rutin). Nevertheless, when natural extracts are being encapsulated, the pH value allows the great amount of RA interaction with CS solution, and then the success of the encapsulation. This means that some phenolic compounds are present in the extracts, but are not negatively charged at formation, medium, and pH, may be lost in the encapsulation procedure. However, other antioxidant compounds in extract nanoparticles that have a close pKa of RA are being encapsulated adding a synergic antioxidant activity. This justifies that with lower RA concentrations, the extracts have the same antioxidant activity, being good vehicles of RA and with good antioxidant synergic performance. Furthermore, it is important to underline that RA-nanoparticles can encapsulate with only 50% of association efficiency, which means a huge waste of the compound. This could represent that at this moment, for all the tests made for CS nanoparticles

with sage or savory, they seem to be good vehicles for RA incorporation and represent a more economically process than nanoparticles with RA pure. Another advantage could be added with the inclusion of biological activities of other natural compounds that were incorporated at this pH value in the nanoparticles. However, *in vitro* tests must be done in order to guarantee that all the biological activities of the extract and of RA are maintained.

Conclusion

The encapsulation of active agents in polymer matrix has demonstrated to benefit from different perspectives, including their protection from the surrounding medium or processing conditions and their controlled release. The antioxidants are sensitive biocompounds against adverse conditions like mucosal enzymes and biological protective fluids. In this study, CS nanoparticles incorporating RA, sage and savory were prepared and characterized in order to ensure their best size, efficient encapsulation, thermal stability, *in vitro* release, and the high antioxidant activity performance.

The core of this work was to underline the potential application of sage and savory for pharmaceutical or biomedical formulations, considering the benefits of natural extracts containing RA. Bearing in mind that natural nanoparticles offer the most advanced treatment modality for crude extracts incorporation. This could be a fundamental alternative nanomedicine to enhanced antioxidant performance for oxidative stress conditions.

Declaration of interest

References

Abada ANA, Nourib MHK, Tavakkolia F. (2011). Effect of *Salvia officinalis* hydroalcoholic extract of vincristine-induced neuropathy in mice. *Chin J Nat Med* 9:0354–8.

Ajun W, Yan S, li G, Huili L. (2009). Preparation os aspirin and probucol in combination loaded chitosan nanoparticles and *in vitro* release study. *Carbohydr Polym* 75:566–74.

Alonso MJ, Sanchéz A. (2003). The potential of chitosan in ocular drug delivery. *J Pharm Pharmacol* 55:1451–63.

Amorim C, Couto A, Netz D, et al. (2010). Antioxidant idebenone-loaded nanoparticles based on chitosan and *n*-carboxymethylchitosan. *Nanomed Nanotech Biol Med* 6:745–52.

Calvo P, Remunan-Lopez C, Vila-Jato JL, Alonso MJ. (1997). Novel hydrophilic chitosan–polyethylene oxide nanoparticles as protein carriers. *J Appl Polym Sci* 63:125–32.

Campos A, Diebold Y, Carvalho E, et al. (2004). Chitosan nanoparticles as new ocular drug delivery systems: *In vitro* stability, *in vivo* fate, and cellular toxicity. *Pharm Res* 21:803–10.

Cardilea V, Russob A, Formisanoc C, et al. (2009). Essential oils of *Salvia bracteata* and *Salvia rubifolia* from Lebanon: Chemical composition, antimicrobial activity and inhibitory effect on human melanoma cells. *J Ethnopharmacol* 126:265–72.

Coneaca G, Gafiţanub E, Hădărugăc N, et al. (2009). Quercetin and rutin/2-hydroxypropyl-β-cyclodextrin nanoparticles: Obtaining, characterization and antioxidant activity. *J Agro Proc Technol* 15:441–8.

Contreras MM, Hernández-Ledesma B, Amigo L, et al. (2011). Production of antioxidant hydrolysates from a whey protein concentrate with thermolysin: Optimization by response surface methodology. *LWT – Food Sci Technol* 44:9–15.

Deladino L, Anbinder PS, Navarro AS, Martino MN. (2008). Encapsulation of natural antioxidants extracted from *Ilex paraguariensis*. *Carbohydr Polym* 71:126–34.

Djenane D, Yangüela J, Montañés L, et al. (2011). Antimicrobial activity of *Pistacia lentiscus* and *Satureja montana* essential oils against *Listeria monocytogenes* cect 935 using laboratory media: Efficacy and synergistic potential in minced beef. *Food Control* 22:1046–53.

Dudhania AR, Kosarajua SL. (2010). Bioadhesive chitosan nanoparticles: Preparation and characterization. *Carbohydr Polym* 81:243–51.

Fadel O, Kirat KE, Morandat S. (2011). The natural antioxidant rosmarinic acid spontaneously penetrates membranes to inhibit lipid peroxidation *in situ*. *Biochim Biophys Acta* 1808:2973–80.

Fujimoto A, Masuda T. (2012). Antioxidation mechanism of rosmarinic acid, identification of an unstable quinone derivative by the addition of odourless thiol. *Food Chem* 132:901–6.

Furtado MA, de Almeida LC, Furtado RA, et al. (2008). Antimutagenicty of rosmarinic acid in Swiss mice evaluated by the micronucleus assay. *Mutat Res* 657:150–4.

Gião M, Pereira C, Fonseca S, et al. (2009). Effect of particle size upon the extent of extraction of antioxidant power from the plants agrimonia eupatoria, *Salvia* sp. And *Satureja montana*. *Food Chem* 117:412–6.

Gião MS, Gonzalez-Sanjose ML, Rivero-Perez MD, et al. (2007). Infusions of Portuguese medicinal plants: Dependence of final antioxidant capacity and phenol content on extraction features. *J Sci Food Agric* 87:2638–47.

Guinesi L, Cavalheiro E. (2006). The use of dsc curves to determine the acetylation degree of chitin/chitosan samples. *Thermochim Acta* 444:128–33.

Hamaguchi T, Ono K, Murase A, Yamada M. (2009). Phenolic compounds prevent Alzheimer's pathology through different effects on the amyloid-beta aggregation pathway. *Am J Pathol* 175:2557–65.

Han L, Du L-B, Kumar A, et al. (2012). Inhibitory effects of trolox-encapsulated chitosan nanoparticles on tertbutylhydroperoxide induced raw264.7 apoptosis. *Biomaterials* 33:8517–28.

Harris R, Lecumberri E, Mateos-Aparicio I, et al. (2011). Chitosan nanoparticles and microspheres for the encapsulation of natural antioxidants extracted from *Ilex paraguariensis*. *Carbohydr Polym* 84:803–6.

Hernández-Ledesma B, Dávalos A, Bartolomé B, Amigo L. (2005). Preparation of antioxidant enzymatic hydrolysates from α-lactalbumin and β-lactoglobulin, identification of active peptides by hplcems. *J Agric Food Chem* 53:588–93.

Hou Y, Wang J, Jin W, et al. (2012). Degradation of *Laminaria japonica fucoidan* by hydrogen peroxide and antioxidant activities of the degradation products of different molecular weights. *Carbohydr Polym* 87:153–9.

Huang H, Hauk C, Yum M-Y, et al. (2009). Rosmarinic acid in *Prunella vulgaris* ethanol extract inhibits lipopolysaccharide-induced prostaglandin e2 and nitric oxide in raw 267.7 mouse macrophages. *J Agric Food Chem* 57:10579–89.

ICH. (2005). *Validation of Analytical Procedures Text and Methodology q2(r1)*. In: International Conference on Harmonisation of Technical Requirements for Registration of Pharmaceuticals for Human Use. Geneva, Switzerland.

Kumari A, Sudesh Y, Pakade Y, et al. (2011). Nanoencapsulation and characterization of *Albizia chinensis* isolated antioxidant quercitrin on pla nanoparticles. *Colloids Surf B* 82:224–32.

Kumari A, Yadav S, Pakade Y, et al. (2010). Development of biodegradable nanoparticles for delivery of quercetin. *Colloids Surf B* 80:184–92.

Lee J, Jung E, Kog J, et al. (2008). Effect of rosmarinic acid on atopic dermatitis. *J Dermatol* 35:768–71.

Liu Y, Sun Y, Li Y, et al. (2011). Preparation and characterization of alpha-galactosidase-loaded chitosan nanoparticles for use in foods. *Carbohydr Polym* 83:1162–8.

Mohanraj VJ, Chen Y. (2006). Nanoparticles: A review. *Trop J Pharm Res* 5:561–73.

Peres I, Rocha S, Gomes J, et al. (2011). Preservation of catechin antioxidant properties loaded in carbohydrate nanoparticles. *Carbohydr Polym* 86:147–53.

Petersen M, Simmonds MSJ. (2003). Molecules of interest: Rosmarinic acid. *Phytochemistry* 62:121–5.

Prabaharan M, Mano JF. (2005). Chitosan-based particles as controlled drug delivery systems. *Drug Deliv* 12:41–57.

Roeges N. (1995). *A Guide to the Complete Interpretation of Infrared Spectra of Organic Structures*. Chichester: Wiley and Sons.

Sarmento B, Ferreira D, Veiga F, Ribeiro A. (2006). Characterization of insulin-loaded alginate nanoparticles produced by ionotropic pregelation through DSC and FTIR studies. *Carbohydr Polym* 66:1–7.

Shahidi F, Yanita PK, Nanosudra PD. (1992). Phenolic antioxidants. *Crit Rev Food Sci* 32:67–103.

Silva SBd, Fernandes J, Tavira F, et al. (2011). The potential of chitosan in drug delivery systems. In: Ferguson AN, O'Neill AG, eds. *Focus on Chitosan Research*. New York: Nova Publishers.

Silva SBd, Oliveira A, Ferreira D, et al. (2013). Development and validation method for simultaneous quantification of phenolic compounds in natural extracts and nanosystems. *Phytochem Anal* 24: 638–44.

Skoula M, Abbes JE, Johnson CB. (2000). Genetic variation of volatiles and rosmarinic acid in populations of *Salvia fruticosa* mill growing in crete. *Biochem Syst Ecol* 28:551–61.

Stehfest K, Boese M, Kerns G, et al. (2004). Fourier transform infrared spectroscopy as a new tool to determine rosmarinic acid *in situ*. *J Plant Physiol* 161:151–6.

Vikas R, Kumar B, Dinesh G, et al. (2004). Optimization of chitosan films as a substitute of animal and human epidermal sheets for *in vitro* permeation of polar and non-polar drugs. *Acta Pharm* 54: 287–99.

Wu T-H, Yen F-L, Lin L-T, et al. (2008). Preparation, physicochemical characterization, and antioxidant effects of quercetin nanoparticles. *Int J Pharm* 346:160–8.

Wu Y, Luo Y, Wang Q. (2012). Antioxidant and antimicrobial properties of essential oils encapsulated in zein nanoparticles prepared by liquideliquid dispersion method. *LWT – Food Sci Technol* 48:283–90.

Xavier CP, Lima CF, Fernandes-Ferreira M, Pereira-Wilson C. (2009). *Salvia fruticosa*, *Salvia officinalis*, and rosmarinic acid induce apoptosis and inhibit proliferation of human colorectal cell lines: The role in maok/erk pathway. *Nutr Cancer* 61:564–71.

Zavatti M, Zanoli P, Benelli A, et al. (2011). Experimental study on *Satureja montana* as a treatment for premature ejaculation. *J Ethnopharmacol* 133:629–33.

Zhoua Y, Lib W, Xua L, Chenc L. (2011). In *Salvia miltiorrhiza*, phenolic acids possess protective properties against amyloid beta-induced cytotoxicity, and tanshinones act as acetylcholinesterase inhibitors. *Environ Toxicol Pharmacol* 31:443–52.